CHAPTER V

SIMULATION

In this chapter , the selected mathematical models of fluid flow in ducts are discretized and totally replaced by a system of algebraic equations which can be solved for the values of the flow-field variables at the discrete points in the domain , or *grid points*.

In the present study , the method of discretization called *finite volume* , is employed via the computer program PHOENICS.

5.1 SOLUTION PROCEDURE

The calculation domain is divided into a finite number of main grid points where pressure and the two turbulence quantities k and ε are stored. The three velocity components $\bar{u}$, $\bar{v}$ and $\bar{w}$ are , on the other hand , stored at grid locations located midway between the main points. The conservation equations are integrated over control volumes surrounding grid points. This integration is performed by application of hybrid-difference scheme and fully-implicit formulation. The result of this is a set of linear algebraic equations which are solved by repeated use of the well known tri-diagonal matrix algorithm along x , y and z directions. Special care has been taken to solve the pressure-velocity coupling of the three momentum equations (4.31) - (4.33) and the mass balance equations (4.21).

The SIMPLE method developed by Patankar and Spalding for three-dimensional parabolic flows has been extended to fully three-dimensional

elliptic flows and is used to solve this coupling (Hjertager and Magnussen , 1981). The method introduces a new variable the socalled pressure correction which makes the necessary corrections to the velocity components to make them obey the continuity constraint. The pressure correction is determined by solution of algebraic equations derived from the linearized momentum equations and the continuity equation.

The algebraic details of the above features can be seen in appendix A : Computational fluid dynamics (CFD) technique.

5.2 GEOMETRY

The numerical solutions are carried out to deepen insight into the flow structure of three-dimensional inclined flat plate flows. A large number of grid points are placed in the areas where steep variation in velocities are expected. A grid density of $N_x \times N_y \times N_z = 5 \times 30 \times 50$ is located in a square duct dimension : $0.15 \times 0.15 \times 7.62$ m and the position of the damper is about 10 diameters behind the inlet off the duct. The inequality of N_x and N_y is resultant of the various geometry cases of the obstacles in the duct and also the computer limitations.

The grid distribution in the calculation domain for x-y plane is uniform for all geometry cases as shown in figure 5.1 , but for y-z plane (the longitudinal coordinate direction) is different as : a blank duct still be uniform grid while 1- , 2- and 3-blade damper cases (for all inclinations of the flat plate) are non-uniform as shown in figures 5.2 , 5.3 , 5.4 and 5.5 respectively.

The acquired numerical results from this simulation can be represented by the straightforward numbers such as the value of mean velocity in z-direction for each x-y plane (see figure 5.6). Moreover , the graphics of the vectors or contours also can be represented (see figure 5.7).

5.3 BOUNDARY CONDITIONS

a) Inlet

- Air density (ρ)   =   1.185   kg / m³.

- Velocity component $\overline{u}$ =   0   m / s.

- Velocity component $\overline{v}$ =   0   m / s.

- Velocity component $\overline{w}$ =   4   m / s.

- At mass-inflow boundaries , the inlet values of kinetic energy of turbulence (k) and rate of dissipation of kinetic energy of turbulence (ε) are usually unknown , and one needs to take guidance from experimental data for similar flows. The simplest practice is to assume uniform values of k and ε computed from

$$k \quad = \quad \left(1 . \overline{w}_{in} \right)^2 \tag{5.1}$$

and $$\varepsilon \quad = \quad \frac{C_{\mu}^{0.75} \; k^{1.5}}{L_{in}} \tag{5.2}$$

where $\overline{w}_{in}$ is the bulk inlet velocity.

I   is the turbulent intensity (= 0.05 or 5 %).

and L_{in} is the inlet mixing length which is estimated to be

$$L_{in} = \frac{0.1 \, D_h}{2} \qquad (5.3).$$

b) Outlet

- External pressure   =   0 N / m^2 .

- No resistance across opening.

- The axial velocity are computed using the nearby velocity distribution and overall continuity requirements.

- The other two velocity components are set equal to zero. The outlet conditions for k and ε are taken to be zero gradient in the z-direction.

c) Walls

- No-slip condition thus $\bar{u} , \bar{v} , \bar{w}$ = 0 m / s along the walls.

- Boundary conditions near the walls have been treated previously in section 4.3 and are not elaborated here.

d) Flat plate

- Fully blocked (value for porosity = 0).

- Wall friction active on both surfaces (front and back).

These informations are the essential parts of the computer command for simulations in this study , however , further details can be seen in appendix B : Computer code.
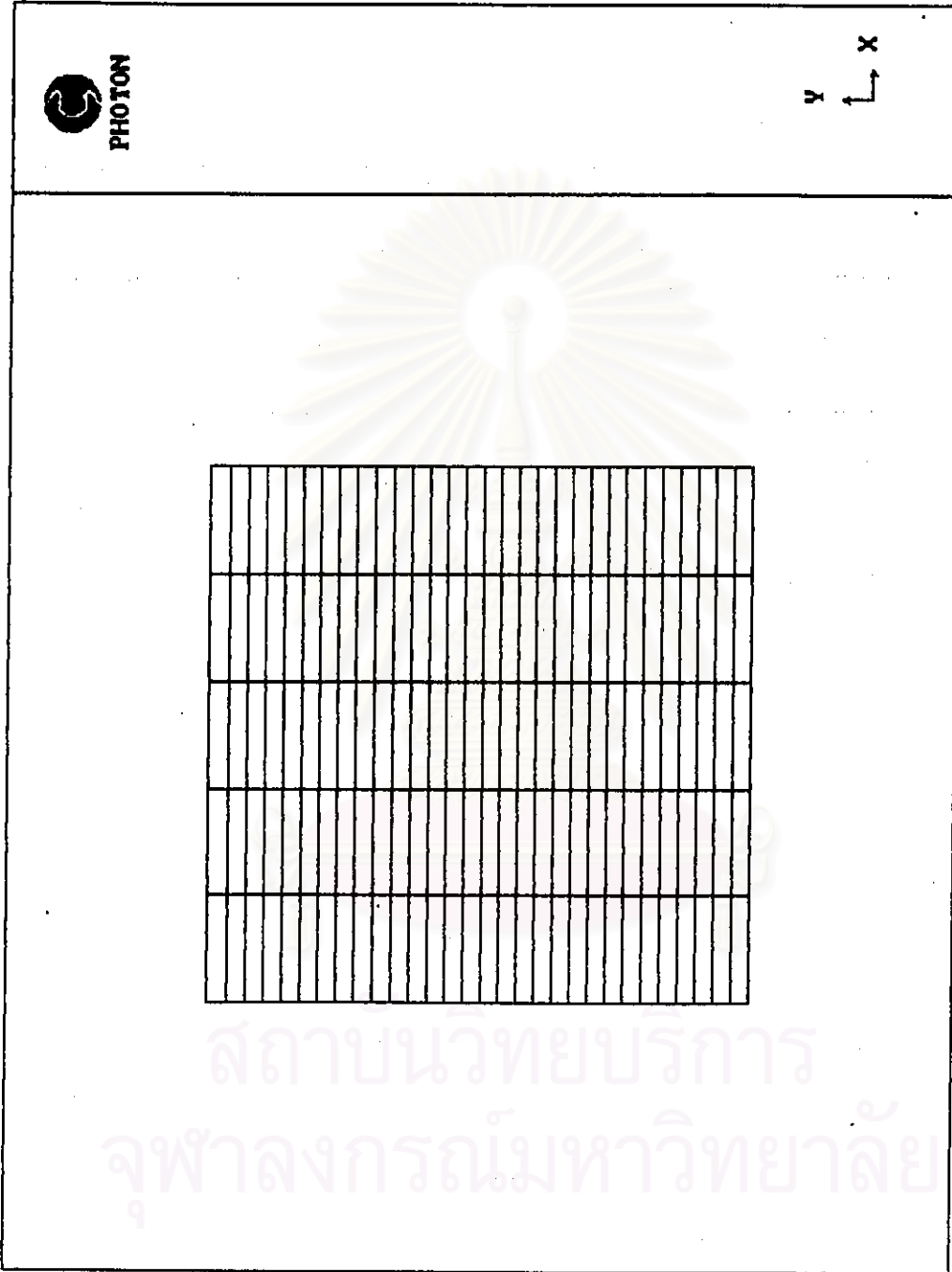
PHOTON

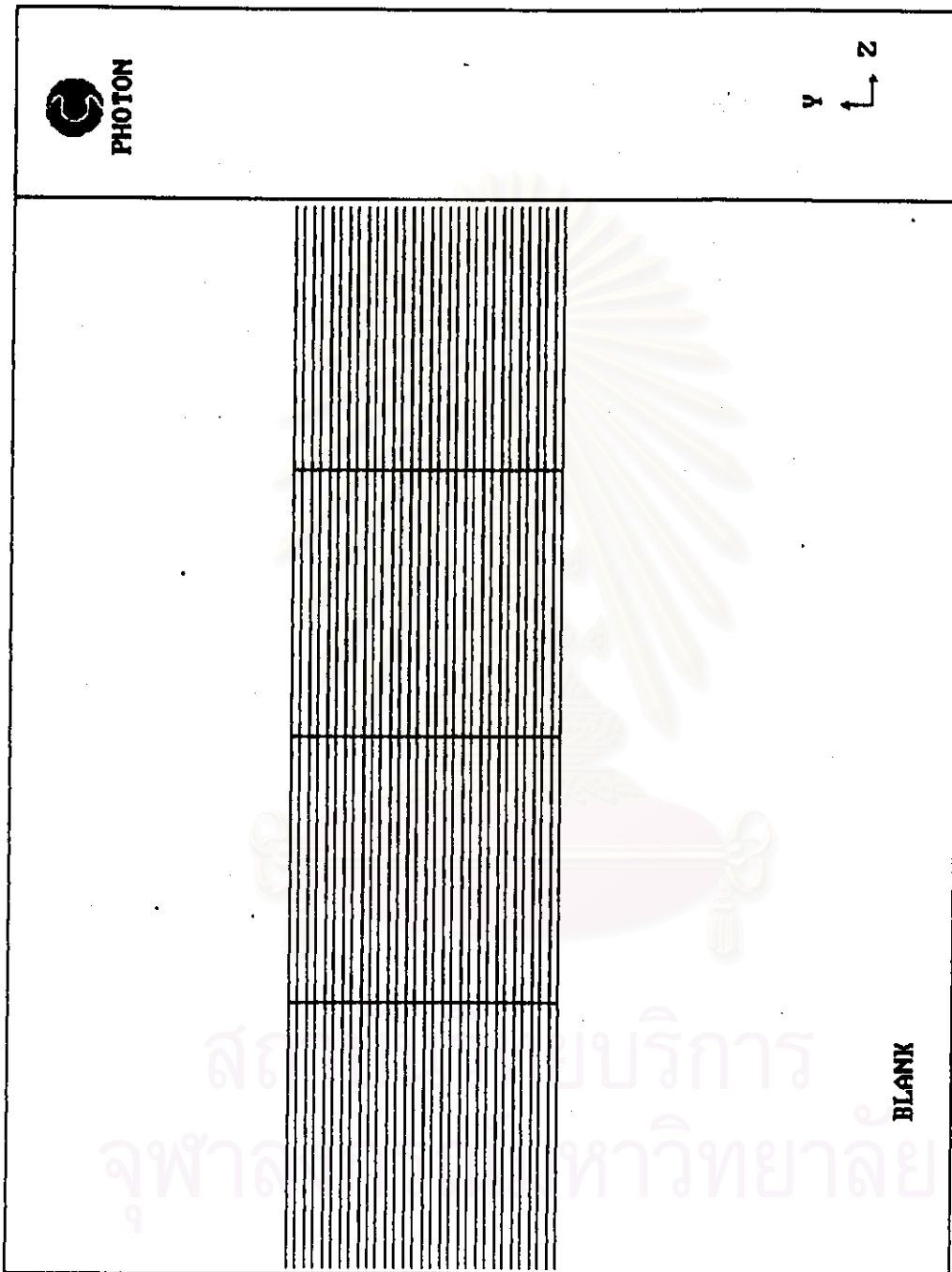Figure 5.1 Grid distribution for x-y plane.

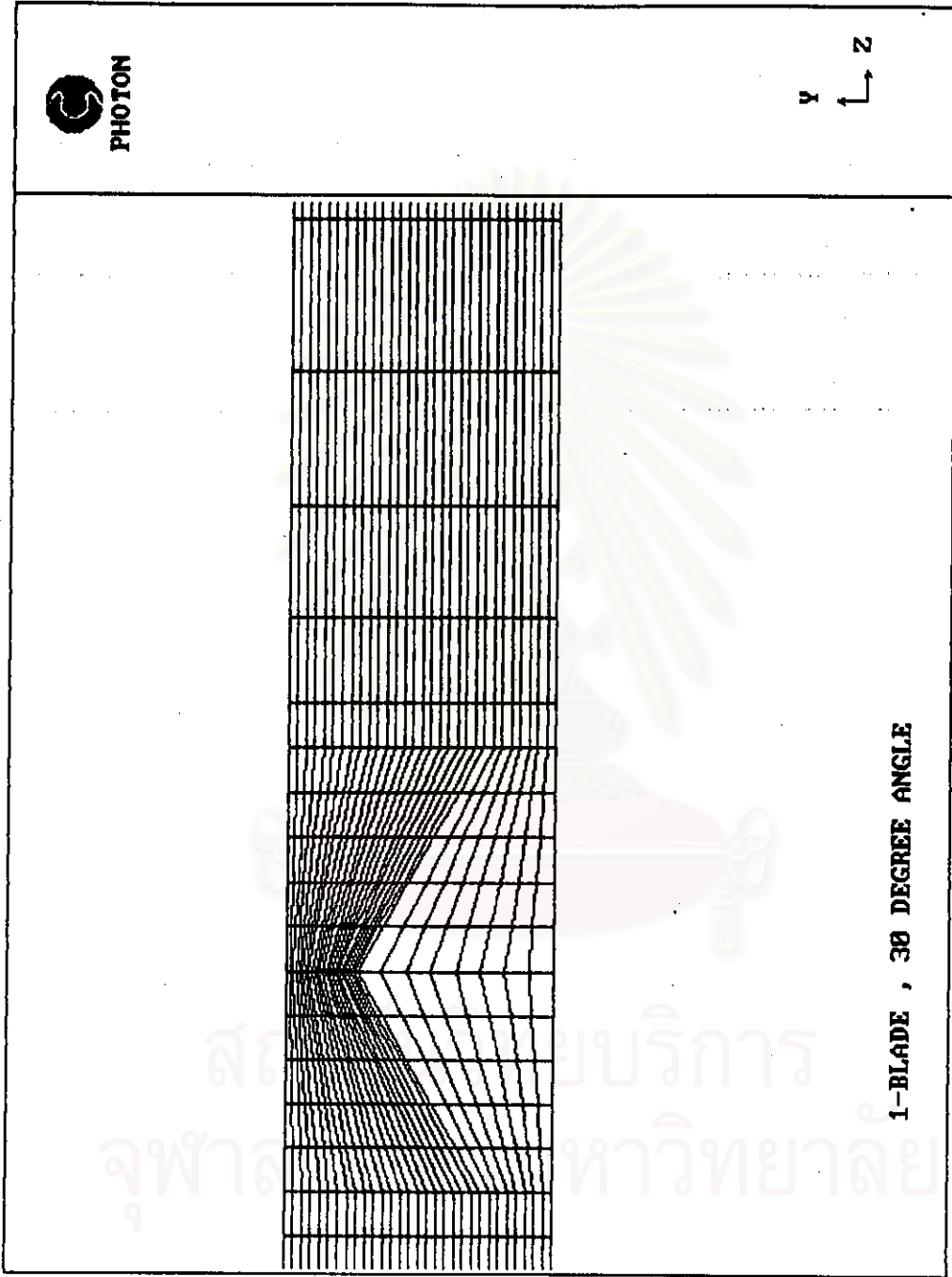Figure 5.2 The numerical grid of air flow in a blank duct for y-z plane.

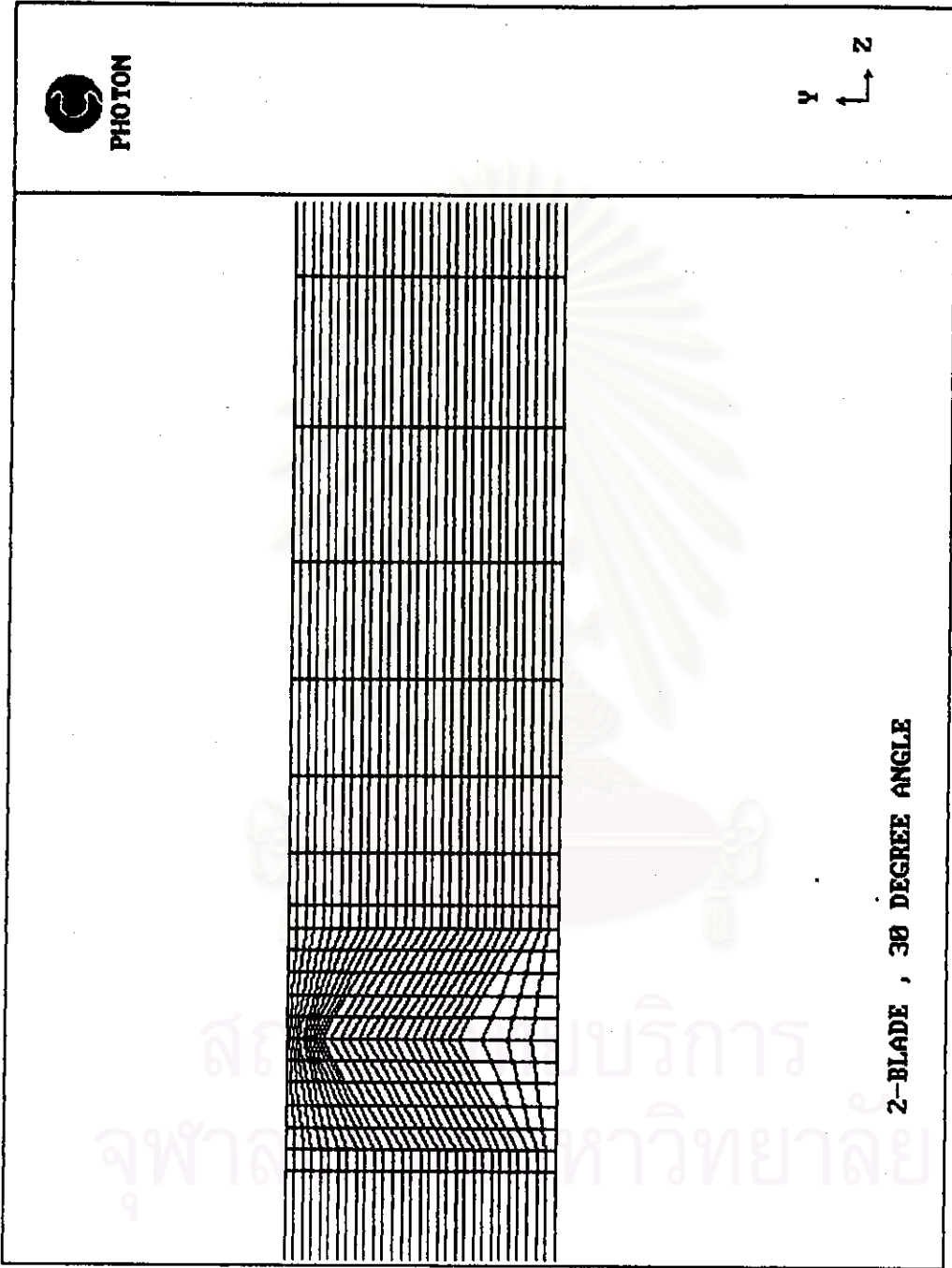Figure 5.3 The numerical grid of air flow past 1-blade damper with 30 degree angle.

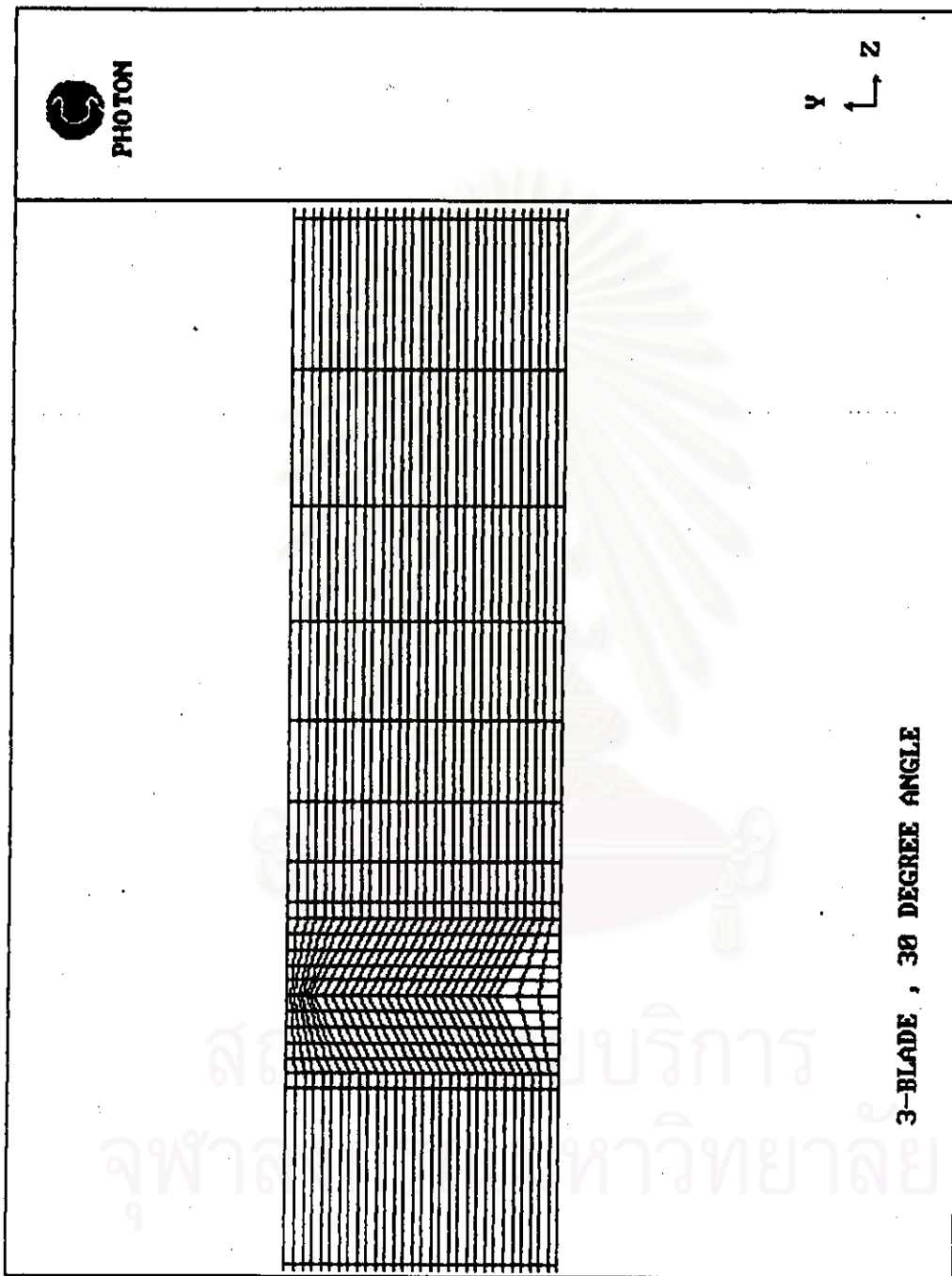Figure 5.4 The numerical grid of air flow past 2-blade damper with 30 degree angle.

Figure 5.5 The numerical grid of air flow past 3-blade damper with 30 degree angle.

```
FLOW FIELD AT ITHYD=    1, IZ=   22, ISWEEP=   3, ISTEP=   1
FIELD VALUES OF W1
```

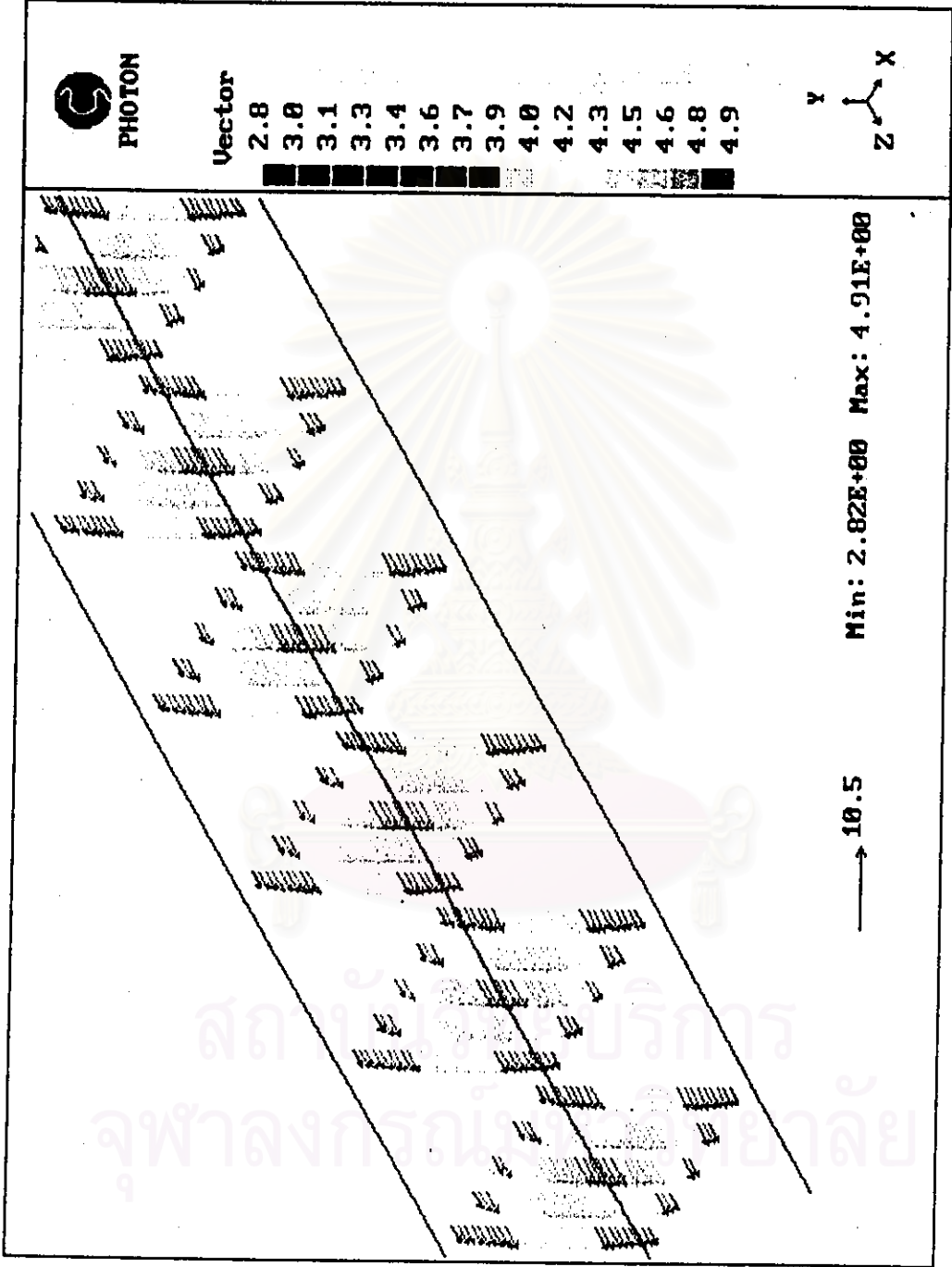| IY=	IX=1	IX=2	IX=3	IX=4	IX=5
30	2.858E+00	2.898E+00	2.954E+00	2.898E+00	2.858E+00
29	3.052E+00	3.443E+00	3.525E+00	3.443E+00	3.052E+00
28	3.222E+00	3.737E+00	3.842E+00	3.737E+00	3.222E+00
27	3.368E+00	3.932E+00	4.061E+00	3.932E+00	3.368E+00
26	3.493E+00	4.077E+00	4.228E+00	4.077E+00	3.493E+00
25	3.599E+00	4.192E+00	4.363E+00	4.192E+00	3.599E+00
24	3.688E+00	4.286E+00	4.476E+00	4.286E+00	3.688E+00
23	3.762E+00	4.364E+00	4.571E+00	4.364E+00	3.762E+00
22	3.822E+00	4.430E+00	4.651E+00	4.430E+00	3.822E+00
21	3.870E+00	4.485E+00	4.718E+00	4.485E+00	3.870E+00
20	3.908E+00	4.529E+00	4.771E+00	4.529E+00	3.908E+00
19	3.937E+00	4.564E+00	4.812E+00	4.564E+00	3.937E+00
18	3.957E+00	4.590E+00	4.840E+00	4.590E+00	3.957E+00
17	3.970E+00	4.607E+00	4.857E+00	4.607E+00	3.971E+00
16	3.977E+00	4.615E+00	4.864E+00	4.615E+00	3.977E+00
15	3.977E+00	4.615E+00	4.864E+00	4.615E+00	3.977E+00
14	3.970E+00	4.607E+00	4.857E+00	4.607E+00	3.971E+00
13	3.957E+00	4.590E+00	4.840E+00	4.590E+00	3.957E+00
12	3.937E+00	4.564E+00	4.812E+00	4.564E+00	3.937E+00
11	3.908E+00	4.529E+00	4.771E+00	4.529E+00	3.908E+00
10	3.870E+00	4.485E+00	4.718E+00	4.485E+00	3.870E+00
9	3.822E+00	4.430E+00	4.651E+00	4.430E+00	3.822E+00
8	3.762E+00	4.364E+00	4.571E+00	4.364E+00	3.762E+00
7	3.688E+00	4.286E+00	4.476E+00	4.286E+00	3.688E+00
6	3.599E+00	4.192E+00	4.363E+00	4.192E+00	3.599E+00
5	3.493E+00	4.077E+00	4.228E+00	4.077E+00	3.493E+00
4	3.368E+00	3.932E+00	4.061E+00	3.932E+00	3.368E+00
3	3.222E+00	3.737E+00	3.842E+00	3.737E+00	3.222E+00
2	3.052E+00	3.443E+00	3.525E+00	3.443E+00	3.052E+00
1	2.858E+00	2.898E+00	2.954E+00	2.898E+00	2.858E+00
IX=	1	2	3	4	5

Figure 5.6 The numerical results for x-y plane.

Figure 5.7 Mean-longitudinal-velocity profiles in three-dimensional flow.